Open-source deep learning-based air-voids detection algorithm for concrete microscopic images

Benoit Hilloulin, Imane Bekrine, Emmanuel Schmitt, Ahmed Loukili

Open-source deep learning-based air-voids detection algorithm for concrete microscopic images

B. Hilloulin[1], I. Bekrine[1], E. Schmitt[2], A. Loukili[1]

[1] Institut de Recherche en Génie Civil et Mécanique (GeM), UMR-CNRS 6183, Ecole Centrale de Nantes, 1 rue de la Noë, 44321 Nantes, France – e-mail: benoit.hilloulin@ec-nantes.fr; imane.bekrine@ec-nantes.fr; ahmed.loukili@ec-nantes.fr

[2] Vicat, 4 rue Aristide Berges – Les trois vallons, 38081 L'Isle d'Abeau, France – e-mail: emmanuel.schmitt@vicat.fr

ABSTRACT.

Analyzing concrete microscopic images is difficult because of its highly heterogeneous composition and the different scales involved. This article presents an open-source deep learning-based algorithm dedicated to air-void detection in concrete microscopic images. The model, whose strategy is presented alongside concrete compositions information, is built using the Mask R-CNN model. Model performances are then discussed and compared to the manual air-void enhancement technique. Finally, the selected open-source strategy is exposed. Overall, the model shows a good precision (mAP=0.6452), and the predicted air void percentage agrees with experimental measurements highlighting the model's potential to assess concrete durability in the future.

KEYWORDS: Concrete; Optical microscopy; Deep learning; Segmentation; Air voids; Digital twin; Open source

1. Introduction

Concrete, the most consumed manufactured material globally, is mainly used in the construction field, because of its low cost and good mechanical and durability properties.

During their life service, concrete constructions are exposed to a variety of harmful environments, in particular, to freeze and thaw cycles in frost regions. Concrete heterogeneous and multi-scale natures are both responsible for its remarkable resistance and its complex behavior against potential degradation. Therefore, characterizing and modeling the multi-scale spatial properties of concrete has attracted attention during the past decades.

For example, air-entrainment using air-entraining agents (AEA) was found to be an effective way to improve freeze-thaw resistance, and the parameters of the entrained air-voids network are to be determined in order to assess its quality. In fact, total air content does not ensure the good protection of concrete alone, and Powers' spacing factor[1] $\bar{L}$ better, representing the maximal distance from any point in the cement paste to the edge of the nearest air-void, matters most. Currently, the most widely used method for the purpose of evaluating this spacing factor is the stereomicroscope-based one described in both ASTM C457 / C457M-16[2] and EN 480-11[3] standards. This manual method is tedious, time-consuming (nearly 3 hours for each slice), and depends on the operator's judgment. In addition, this method may not be representative of the real air-void structure since the measurements are one-dimensional. Other techniques have been used to overcome some of the limitations of the standard methods. For example, X-ray micro-computed tomography can give the spatial 3D air-void structure[4]. The manual segmentation technique of 2D enhanced contrast images, either between aggregates and paste by using phenolphthalein or between air-voids and the rest of the constituents by black inking the surface and filling the air voids with white powder can also be used[5,6]. The automated air-void analyzer RapidAir 457 can also help inspect black inked surfaces[7]. Nonetheless, all these methods are not entirely automatized and the uncertainties brought by operator interference and subjectivity may be a source of significant errors.

Due to the complex heterogeneous nature of concrete, phase separation remains a challenging task. The last advances in machine learning led to a better understanding of concrete properties,

from strength[8] to shrinkage[9] or micro-mechanical properties[10], and, more specifically, deep learning segmentation techniques have been fruitful in different fields[11]. For visual imagery, a convolutional neural network (CNN) might be used, combined with other techniques, to increase observation precision classifying or detecting objects of low contrast with a completely automated procedure. In terms of concrete petrographic analysis, the outcomes are not yet well studied because of the lack of information for validation steps. Yet, it recently showed a promising potential for crack damage detection and monitoring[12–14] in concrete, some defaults in different structures[15,16] and air voids detection[17].

The aim of the current study is to address the challenge of fast and accurate air-void analysis of concrete with the minimum amount of sample preparation and human bias-prone preparation and interpretation. To this end, an open-source deep learning-based air-voids detection algorithm for concrete microscopic images is introduced. The principle of the model is first presented and then some of its advantages are given and finally the open-source code architecture is presented.

2. Materials and methods

2.1 Concrete formulations

Several concrete samples were employed in this study, divided into two sets. The first one was used for the model training and involved concrete samples of different air void structures and a wide variety of aggregates nature (calcareous/siliceous) and size distributions; in order to get the model well trained. . The other set of samples was used for the validation of the analysis method: different dosages of AEA were used ranging from 0.05% to 0.13% of cement weight in order to get concretes with different air-voids structures. Some of these mix proportions were used to formulate different concretes changing just the cement type. Table 1 summarizes the

77 composition of this second set of concrete samples. The nature of superplasticizers 1 and 2
78 cannot be revealed for confidentiality purposes.

79 *2.2 Experimental testing and microscopic measurements*

80 For this validation set of concrete samples, the amount of entrained air was measured on fresh
81 concrete samples according to NF EN 12350-7 standard.

82 Prior to microscopic analysis, special care was given to the sample preparation step in order to
83 get good quality images for microscopic analyses and clearly distinguish phases for the manual
84 method. For each formulation, two 10x10x2 cm^3 slices were cut from 15x15x15 cm^3 cubic
85 concrete samples, in a way that keeps parallel the two faces of the slice; and then they were
86 polished using different SiC papers of decreasing grit sizes to minimize surface defects. The
87 quality of the surface is checked after each polishing step. On each prepared surface, the spacing
88 factor $\bar{L}$ has been evaluated using the point-count method of the manual petrography test method
89 described in ASTM C457 / C457M-16 standard.

90 Concrete microscopic images were obtained using a Hirox RH-2000 3D microscope. A
91 magnification of x50 was used in the image acquisition, which is the same as the required one
92 in the ASTM C457 / C457M-16 standard in order to allow proper comparison; this led to 3.13
93 µm pixel size. Several 768 (H) ×480 (V) pix images, approx.. 7000 to 8000 in total, have been
94 acquired and merged with a 1/2 relative overlap to reconstruct an 8x8 cm^2 image with a 3.13
95 µm resolution.

96 *2.3 Manual contrast enhancement of sections and model comparison.*

97 The classic black and white contrast enhancement method has been used for some sections after
98 the raw image acquisition for comparison purposes of the proposed CNN-based method to
99 standard methods. Contrast enhancement was achieved by drawing slightly overlapping parallel
100 lines with a wide-tipped black permanent marker. This was done in three coats, changing the

orientation by 90° between coats. After the ink dried, a few tablespoons of thin-sized white powder were worked into the samples using the flat face of a glass slide. A razor blade was used to scrape excess powder, leaving powder pressed into voids. The residual powder was removed by wiping with a clean and lightly oiled fingertip. A fine-tipped black marker was used to darken voids in aggregates and cracks.

2.4 Instance segmentation algorithm

An instance segmentation algorithm was built in order to perform segmentation based on Mask R-CNN as illustrated in Fig. 1 to detect air voids in high definition microscopic concrete images. To train the model, 1470 images with equivalent magnifications ranging from × 10 to × 100 and a 608 pix × 608 pix size were selected from various cement paste, mortar and concrete samples. This dataset was divided into training, validation, and test sets given the following proportions: 78%, 13%, 9%. All the images were annotated using VGG Image Annotation software. The training was performed during 600 epochs (250 steps/epoch) on a commercial GPU (Nvidia RTX 2080 Ti, 11 Go GDDR6) using initial weights from COCO dataset. Bitmap images were then built using the predictions from the high and the reduced definition image by selecting the minimum intensity for each pixel as explained in Fig. 1 b). Finally, an air-voids map has been generated and can be compared to images obtained through manual contrast enhancement as described in the previous sub-section. The comparison procedure between the numerical and the experimental air voids maps is illustrated in Fig. 1 b). Model performance has been validated the mean average precision and the intersection over union (IoU) indicators. mAP can be defined as follows:

$$mAP = \frac{\sum_{q=1}^{Q} AveP(q)}{Q} \quad (1)$$

where Q is the number of queries in the set and $AveP(q)$ is the average precision (AP) for a given query, q.

3. Results and discussion

3.1 Model performance

The mean average precision (mAP) of the model was found to be 0.6452 and the IoU ranged from 0.810 to 0.890 on test images. Thus, the very high precision of the air void detection model is comparable to the precision obtained on large datasets in international competitions for common objects detection[18].

The model has then been applied on completely unknown large-scale high-definition images of concretes whose formulations are given in Table 1. The comparison between the predicted and the manual air-void structure analysis can be analyzed as illustrated in Fig. 2. The algorithm successfully detected air voids and air void maps can be obtained as illustrated in Fig. 2 a). The air content associated with the model prediction equaled 7.76 % (1706 air voids) which is close to the fresh state measured air void content (7.4 %) and the air content measured using ASTM C457 / C457M-16 method which is 7.94 %. However, the manually calculated air void content of the concrete based on Fig. 2 b) image is around 12.8 % (1327 detected air voids) which is higher than the predicted air void content and the measured fresh state air void content.

Therefore, the model results are closer to the experimentally measured values than the classically manually colored image analysis technique which constitutes a very promising feature regarding its industrial application. The difference between these values can be attributed to several phenomena: first, the preparation of slices is a critical step and often leads to the overestimation of the actual air void content as some powder particles may be stuck in non perfectly flat regions such as asperities on aggregates, second, the CNN model is less error-prone, and its results are reproducible, which is not the case in experimental samples preparation.

149 *3.2 Open-source code availability and website deployment*

150 Source code is available on a GitLab instance[19]. Code has been divided between the training
151 procedure and the files related to detection on concrete images (image split, model inference
152 and final image merge). Once public, all the contributions to the source code will be allowed.
153 The open-source strategy of the model is given in Fig. 3. The user can run the source code using
154 its own image and a Python interpreter (Option A). In the future, a dedicated website might be
155 implemented to facilitate the inference (Option B).

156

157 **4. Conclusions**

158 In this article, an open-source deep learning instance segmentation model has been developed
159 to detect air voids in cementitious materials using uncolored slices and without any other human
160 intervention (except during the polishing step). Based on the state-of-the-art Mask R-CNN
161 model with a Resnet-101 backbone architecture, the model has been trained to accurately detect
162 air voids with a circular or an irregular shape within a wide range of cementitious materials.
163 The principle of the model has been presented, and its performance has been quantified. The
164 main results can be summarized as follows:

165 - The adapted Mask R-CNN model has then been trained using various concrete and
166 mortar training images on a commercial GPU
167 - Thousands of air voids can be easily detected with the model in some minutes and clear
168 boundaries can be drawn between the instances
169 - The detection of pores on large-scale concrete sections has been performed with good
170 precision (mAP=0.6452) using a novel strategy combining the model results on full-
171 size images and reduced-size images

- The model predictions agree with the experimentally measured fresh-state air content, while air void content can be overestimated using the manual contrast enhancement method.

References

1. Powers TC, Willis TF (1950) THE AIR REQUIREMENT OF FROST RESISTANT CONCRETE. *Highway Research Board Proceedings* **29**. Available at: https://trid.trb.org/view/101611 [Accessed July 12, 2021].

2. ASTM C457 / C457M-16 (2016) Standard Test Method for Microscopical Determination of Parameters of the Air-Void System in Hardened Concrete.

3. EN 480-11 (2005) Admixtures for concrete, mortar and grout. test methods. Determination of air void characteristics in hardened concrete.

4. Kim KY, Yun TS, Choo J, Kang DH, Shin HS (2012) Determination of air-void parameters of hardened cement-based materials using X-ray computed tomography. *Construction and Building Materials* **37**, 93–101.

5. Peterson KW, Swartz RA, Sutter LL, Van Dam TJ (2001) Hardened Concrete Air Void Analysis with a Flatbed Scanner. *Transportation Research Record* **1775**, 36–43.

6. Peterson K, Carlson J, Sutter L, Van Dam T (2009) Methods for threshold optimization for images collected from contrast enhanced concrete surfaces for air-void system characterization. *Materials Characterization* **60**, 710–5.

7. Jakobsen UH, Pade C, Thaulow N, Brown D, Sahu S, Magnusson O, De Buck S, De Schutter G (2006) Automated air void analysis of hardened concrete — a Round Robin study. *Cement and Concrete Research* **36**, 1444–52.

8. Lyngdoh GA, Zaki M, Krishnan NMA, Das S (2022) Prediction of concrete strengths enabled by missing data imputation and interpretable machine learning. *Cement and Concrete Composites* **128**, 104414.

9. Hilloulin B, Tran VQ (2022) Using machine learning techniques for predicting autogenous shrinkage of concrete incorporating superabsorbent polymers and supplementary cementitious materials. *Journal of Building Engineering* **49**, 104086.

10. Hilloulin B, Lagrange M, Duvillard M, Garioud G (2022) ε–greedy automated indentation of cementitious materials for phase mechanical properties determination. *Cement and Concrete Composites (in press)*.

11. Minaee S, Boykov YY, Porikli F, Plaza AJ, Kehtarnavaz N, Terzopoulos D (2021) Image Segmentation Using Deep Learning: A Survey. *IEEE Transactions on Pattern Analysis and Machine Intelligence*, 1–1.

12. Cha Y-J, Choi W, Büyüköztürk O (2017) Deep Learning-Based Crack Damage Detection Using Convolutional Neural Networks. *Computer-Aided Civil and Infrastructure Engineering* **32**, 361–78.

13. Choi W, Cha Y-J (2020) SDDNet: Real-Time Crack Segmentation. *IEEE Transactions on Industrial Electronics* **67**, 8016–25.

14. Kim B, Cho S (2019) Image-based concrete crack assessment using mask and region-based convolutional neural network. *Structural Control and Health Monitoring* **26**, e2381.

15. Amhaz R, Chambon S, Idier J, Baltazart V Automatic Road Crack Detection Based on a Shortest-Path Algorithm, in IEEE Transactions on Intelligent Transportation Systems, vol. 17, no. 10, pp. 2718-2729, Oct. 2016, doi: 10.1109/TITS.2015.2477675

16. Xue Y, Jia F, Cai X, Shadabfar M, Huang H (2022) An optimization strategy to improve the deep learning-based recognition model of leakage in shield tunnels. *Computer-Aided Civil and Infrastructure Engineering* **37**, 386–402.

17. Song Y, Huang Z, Shen C, Shi H, Lange DA (2020) Deep learning-based automated image segmentation for concrete petrographic analysis. *Cement and Concrete Research* **135**, 106118.

18. He K, Gkioxari G, Dollár P, Girshick RB (2017) Mask R-CNN. In: *2017 IEEE International Conference on Computer Vision (ICCV)*, Venice (Italy), pp 2980–8.

19. Hilloulin B (2021) Concrete Deep Segmentation. Available at: https://git.gem.ec-nantes.fr/bhilloul/concrete-deep-segmentation [Accessed March 10, 2022].

228 **Table 1.** Mix proportion of concrete validation set (kg/m^3)

Cement	Sand 0/4	Gravel 4/10	Gravel 10/20	Water	Admixture 1	Admixture 2	AEA	w/c
385	795	244	701	171	3.08	0.963	0.501	0.42
385	795	244	701	171	3.08	0.963	0.193	0.42
385	795	245	701	181	3.08	0.963	0.231	0.42
350	880	918	-	162	2.275	0.350	0.420	0.44
385	850	289	640	169	1.925	-	0.270	0.45

229

230

a)

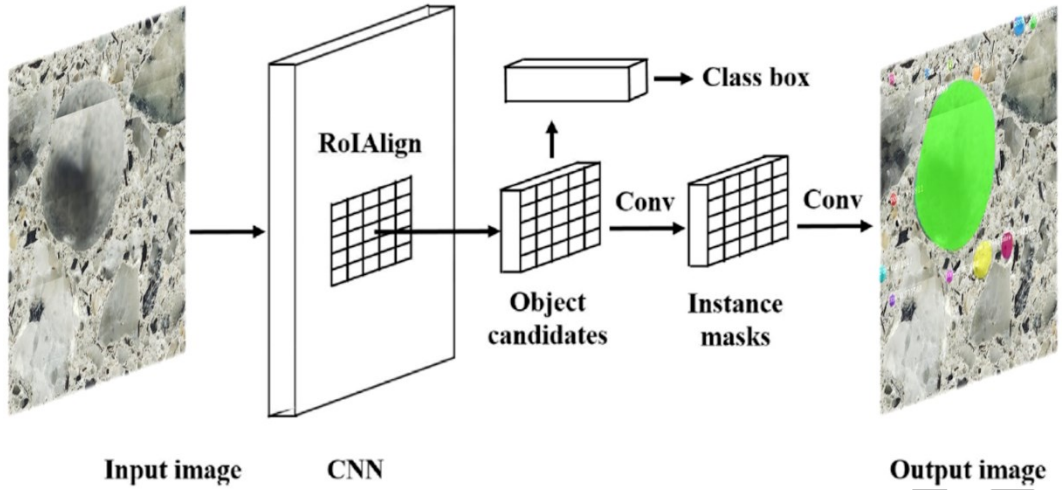

b)

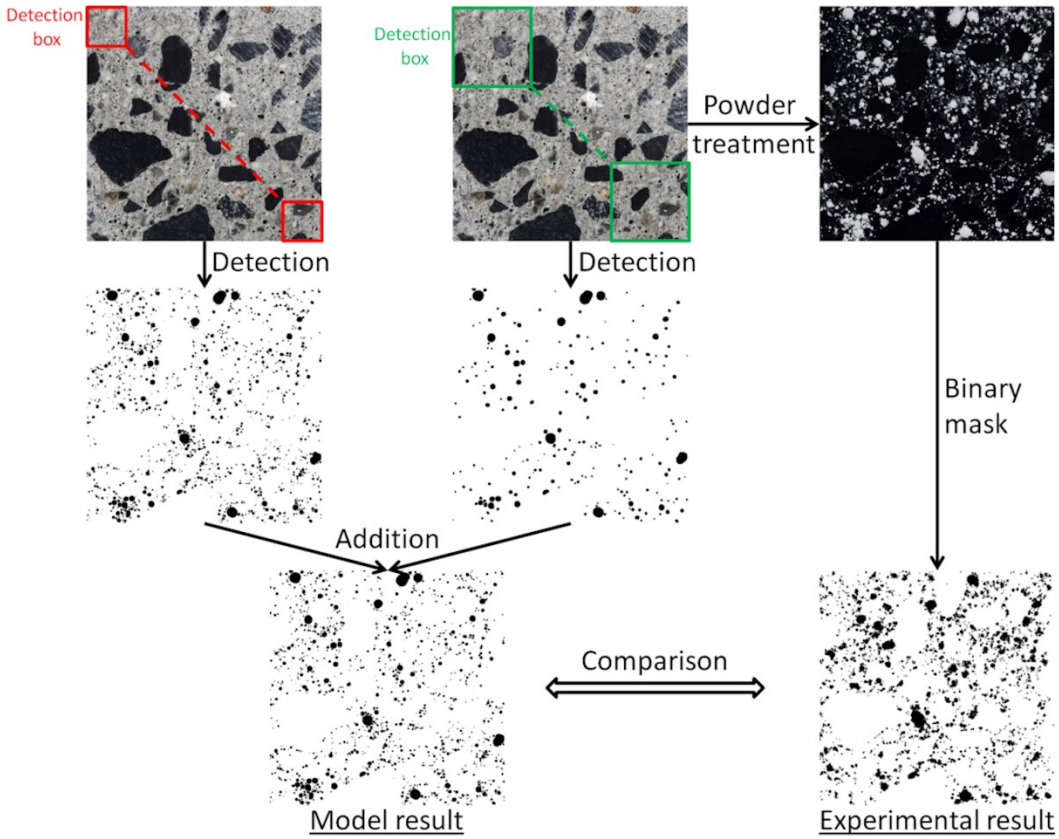

231 **Fig. 1.** Deep Learning air void detection algorithm: a) adapted Mask R-CNN architecture, b) inference

232 strategy on large-scale concrete images and comparison with powder-treated sections.

233

a)

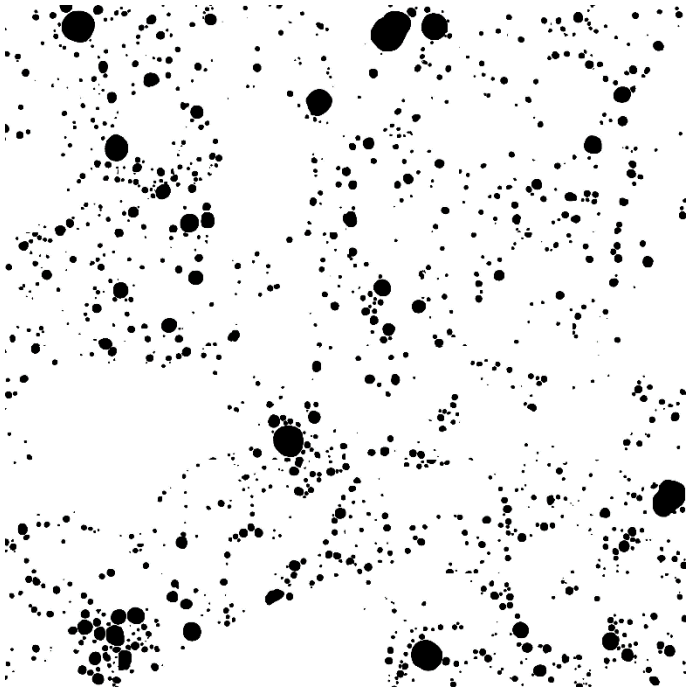

b)

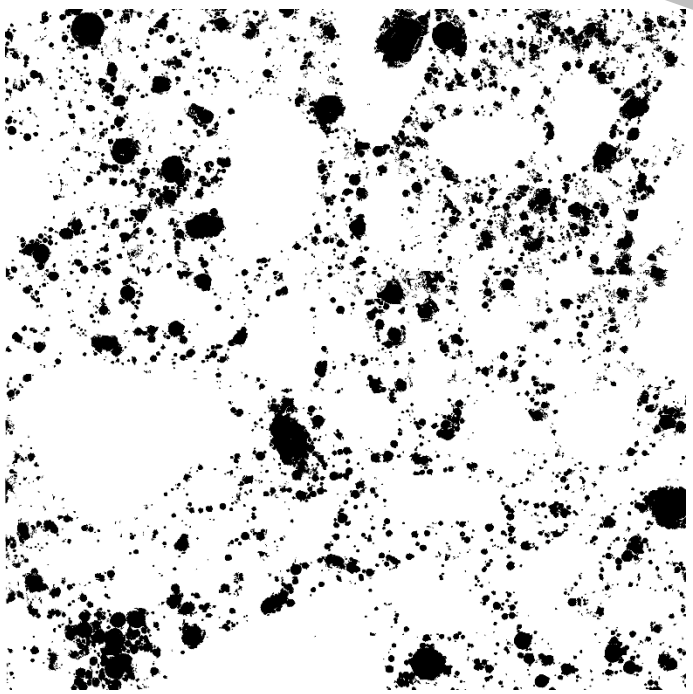

234 **Fig. 2.** Comparison example of the model to manual air void image analysis: a) binary image of the
235 added predictions on the full-size image and on the reduced-size image, b) binary image of the voids
236 detected using the manual analysis.

237

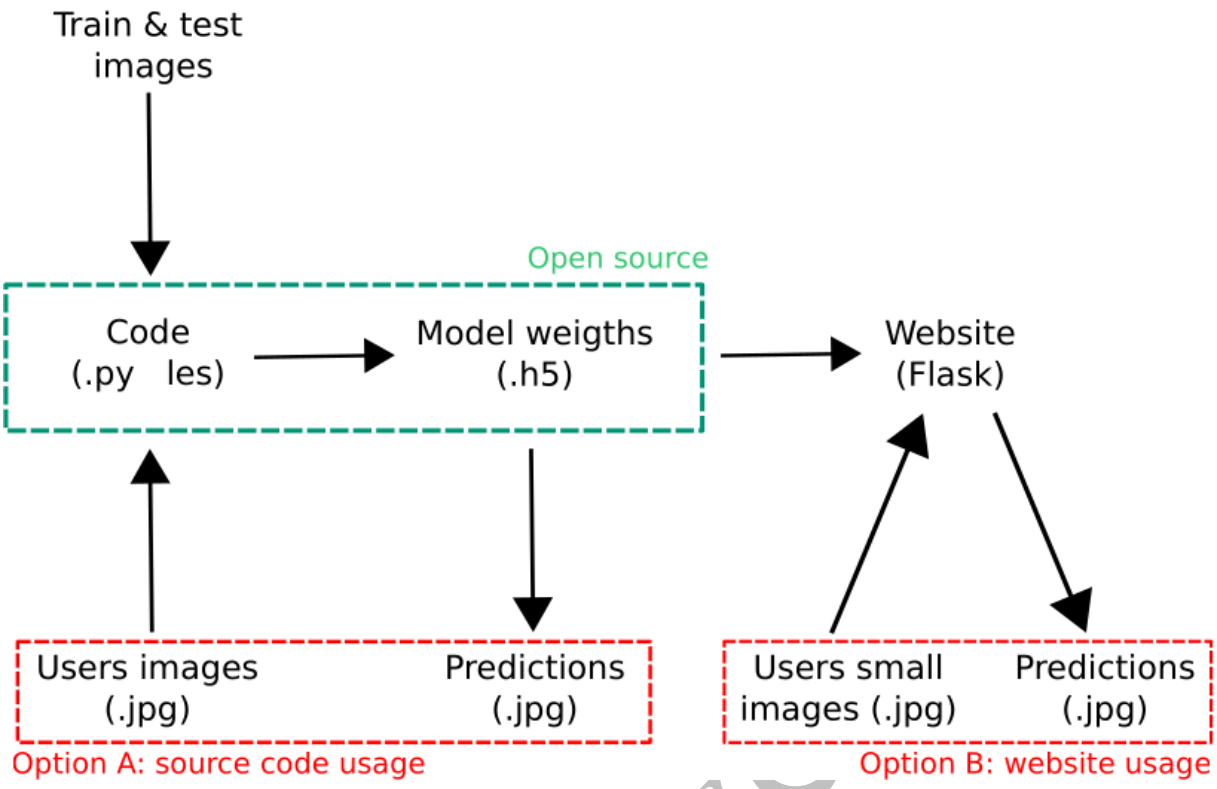

Fig. 3. Open-source code availability and associated usage options.